Crystal and Molecular Structure, Magnetic Properties and Scattered-wave Description of the Electronic Structure of the Hexanuclear Octahedral Clusters $[Fe_6(\mu_3\text{-}S)_8(PEt_3)_6][PF_6]_n$ ($n = 1$ or 2)†

Alessandro Bencini,*[a] Carlo A. Ghilardi,[b] Stefano Midollini,*[b] Annabella Orlandini,[b] Umberto Russo,[c] Myriam G. Uytterhoeven[a] and Claudia Zanchini[d]

[a] *Dipartimento di Chimica, Università di Firenze, Firenze, Italy*

[b] *ISSECC, C.N.R., Firenze, Italy*

[c] *Dipartimento di Chimica, Università di Padova, Padova, Italy*

[d] *Dipartimento di Chimica, Università della Calabria, Arcavacata di Rende (CS), Italy*

The crystal structure of $[Fe_6(\mu_3\text{-}S)_8(PEt_3)_6][PF_6]_2$ has been determined. It is isostructural with the parent tetraphenylborate complex. The electronic structures of $[Fe_6(\mu_3\text{-}S)_8(PEt_3)_6][PF_6]$ and of $[Fe_6(\mu_3\text{-}S)_8(PEt_3)_6][PF_6]_2$ have been investigated experimentally by measuring the temperature variation of the magnetic susceptibility between 300 and 4.2 K, the field dependence of the magnetisation at three different temperatures in the range 2–10 K and the polycrystalline powder Mössbauer spectra at variable temperature. The complex $[Fe_6(\mu_3\text{-}S)_8(PEt_3)_6][PF_6]$ possesses a $S = \frac{1}{2}$ spin state well isolated from the excited states, while $[Fe_6(\mu_3\text{-}S)_8(PEt_3)_6][PF_6]_2$ shows a marked temperature dependence of the magnetic susceptibility. The magnetic structures of the complexes have been characterised empirically with the Heisenberg–Dirac–van Vleck exchange spin Hamiltonian. The nature of the magnetic states is rationalised in the framework of Xα-SW theory.

The synthesis and characterisation of chalcogenide clusters of transition metals is an important topic in modern chemistry.[2] Apart from cubane-like complexes, which have been studied extensively, a number of other structures can be obtained. For example, clusters containing a core formed by an almost perfect octahedron of metals can be obtained by reacting inorganic chalcogenides with the appropriate transition metals in the presence of triethyl- or triphenyl-phosphine.[2] Most of the compounds obtained so far contain the metals in low-spin states and are paramagnetic. The interpretation of their magnetic behaviour is by no means obvious, but important, since these systems can be considered as bridges[3] between simple paramagnets, in which magnetic moments are isolated at a molecular level, and ordered magnetic solids, in which long-range electron correlation occurs. The properties of these latter systems are currently being investigated in view of possible applications as magnetic materials.[4] Spin-dependent electronic delocalisation is also likely to occur, since non-integer oxidation states on the metals are easily obtained. A link can, therefore, be established with biological systems,[5] like iron–sulfur proteins, in which electron delocalization plays a major role in their catalytic activity.

Recently we have reported[6] the interpretation of the redox and magnetic properties of the cobalt clusters $[Co_6(\mu_3\text{-}S)_8(PEt_3)_6]^{0,+}$, where only the cation is paramagnetic and contains one unpaired electron. This unpaired electron has been found to be delocalised over the whole cluster depending on the actual crystallographic symmetry, which is mainly imposed by the nature of the counter anion.[7] Iron clusters isostructural with the cobalt ones have been reported previously.[2] The magnetic properties of $[Fe_6(\mu_3\text{-}S)_8(PEt_3)_6][BPh_4]_2$ were studied in 1985[8] by measuring the temperature dependence of the magnetic susceptibility from room temperature to 77 K. Upon decreasing the temperature to 4.2 K a plateau in the χT *vs.* T curve was obtained[1] in the temperature range 70–60 K. The observed magnetic behaviour is indicative of the presence of magnetic states separated from the ground state by an amount of energy of the order of kT. This situation is usually found in transition-metal oligonuclear complexes[9] and it is often referred to as a weak-bonding interaction. Phenomenologically the relative energies of the spin states are accounted for by using the Heisenberg–Dirac–van Vleck exchange Hamiltonian[10] which reduces the electron–electron interactions to formal coupling between magnetic moments. The rationalisation of the magnetic behaviour of $[Fe_6(\mu_3\text{-}S)_8(PEt_3)_6][BPh_4]_2$ came from density functional calculations[11] performed in the Xα-SW approximation.[12,13] These calculations showed[1] that the maximum spin state compatible with the electronic structure of the cluster was $S = 4$. This spin state can arise from the magnetic coupling between five low-spin ($S_i = \frac{1}{2}$) and one intermediate-spin ($S_j = \frac{3}{2}$) iron(III) centres. Quantitative agreement with experiment was obtained using this model. The anomaly in the χT *vs.* T curve was attributed to a phase transition or to a spin transition of iron(III) from the intermediate to the low-spin value. Although this picture cannot completely account for the electronic structure of the cluster, as it does not take into account the equivalence between the iron centres seen in the crystal structure, it allows a simple rationale for the magnetic properties of $[Fe_6(\mu_3\text{-}S)_8(PEt_3)_6][BPh_4]_2$ and we suggested this molecule is called a mixed-spin-state complex.[1]

In order to obtain more insight into the electronic structure

† Electronic Structure of Paramagnetic Clusters of Transition-metal Ions. Part 4.[1]

Supplementary data available: see Instructions for Authors, *J. Chem. Soc., Dalton Trans.*, 1995, Issue 1, pp. xxv–xxx.

Non-SI units employed: eV ≈ 1.60×10^{-19} J, $\mu_B \approx 9.274 \times 10^{-24}$ J T^{-1}, emu = SI × $10^6/4\pi$.

and redox properties of these clusters, and, in particular, to investigate the possible effect of solid-state interactions we have resorted to synthesizing clusters having the same arrangement of metal ions, but which crystallise with different counter ions, and clusters with chalcogenides other than S. The synthesis of the monopositive iron cation has been reported and the crystal structure of its hexafluorophosphate salt, $[Fe_6(\mu_3\text{-}S)_8(PEt_3)_6][PF_6]$ **1**, determined.[14] We have prepared the hexafluorophosphate salt of the dipositive cation cluster, $[Fe_6(\mu_3\text{-}S)_8(PEt_3)_6][PF_6]_2$ **2**, and report here a full characterisation of the electronic structure and magnetic properties of both complexes **1** and **2**. In order to measure the influence of the counter ion and of inter-cluster interactions on the magnetism of the dipositive cation, we also report the crystal-structure determination of complex **2**. The physicochemical properties of **1** and **2** have been investigated through magnetisation measurements and, for **1**, Mössbauer spectroscopy. The bonding in these complexes is discussed within the Xα-SW formalism which has proved to be useful in the characterisation of transition-metal oligonuclear complexes.[5,15,16]

Experimental and Computational

Synthesis of Complex **2**.—Complex $[Fe_6(\mu_3\text{-}S)_8(PEt_3)_6][PF_6]_2$ **2** was prepared following the procedure previously reported[8] for $[Fe_6(\mu_3\text{-}S)_8(PEt_3)_6][BPh_4]_2$ using tetrabutylammonium hexafluorophosphate instead of sodium tetraphenylborate. Yield 20% (Found: C, 26.9; H, 5.4; Fe, 21.4. Calc.: C, 27.2; H, 5.7; Fe, 21.1%).

X-Ray Data Collection and Reduction.—The procedure followed for data collection and processing was as described elsewhere,[14] and the intensities were corrected following the procedure reported previously.[17,18] Crystal data and data collection details for $[Fe_6(\mu_3\text{-}S)_8(PEt_3)_6][PF_6]_2$ **2** are given in Table 1.

The structure was solved by the heavy-atom method and refined by full-matrix least squares minimising the function $\Sigma w(|F_o| - |F_c|)^2$, with $w = 1/\sigma^2(F_o)$. Atomic scattering factors for the non-hydrogen and hydrogen atoms were taken from refs. 19 and 20 respectively. An anomalous dispersion correction, with real and imaginary parts, was applied in the F_c calculations.[21] Anisotropic thermal parameters were assigned to the iron, sulfur and phosphorus atoms. Hydrogen atoms were introduced in their calculated positions, but were not refined. All calculations were performed on a PC 486 HP, using SHELX 76[22] and ORTEP.[23] Final atomic parameters are given in Table 2.

Additional material available from the Cambridge Crystallographic Data Centre comprises H-atom coordinates, thermal parameters and remaining bond lengths and angles.

Magnetic Measurements.—The temperature dependence of the magnetic susceptibility of $[Fe_6(\mu_3\text{-}S)_8(PEt_3)_6][PF_6]_2$ **2** was measured in the temperature range 6–280 K by the Faraday method using an AZTEC Informatique automated magnetometer equipped with an Oxford Instruments CF2000 cryostat. All other magnetic measurements were performed with a Metronique Ingenierie SQUID susceptometer.

Mössbauer Spectra.—The Mössbauer spectra were obtained in a conventional constant-acceleration spectrometer operating in the horizontal transmission mode which utilised a room-temperature rhodium matrix cobalt-57 source and was calibrated at room temperature with natural abundance α-iron foil. All measurements were performed in a liquid-helium TBT cryostat equipped with a variable-temperature sample holder. The spectroscopic parameters were obtained by least-squares fit of Lorentzian lines to the experimental data.

Xα-SW Calculations.—The Xα-SW calculations were performed on the model molecule $[Fe_6(\mu_3\text{-}S)_8(PH_3)_6]^{n+}$ ($n = 0$, 1, 2, 3 or 4), where the triethylphosphine ligands are replaced by phosphines. The overall symmetry of the cluster is idealised to D_{3d} by making all the Fe–S and Fe–P bonds equivalent. This symmetry is higher than that actually observed in the crystal structure of $[Fe_6(\mu_3\text{-}S)_8(PEt_3)_6][PF_6]$ **1**, point symmetry S_6, and is necessary to avoid the use of complex basis functions.

Table 1 Crystallographic and data collection parameters for $[Fe_6(\mu_3\text{-}S)_8(PEt_3)_6][PF_6]_2$ **2**

Formula	$C_{36}H_{90}F_{12}Fe_6P_8S_8$
M	1590.48
Crystal size/mm	0.25 × 0.25 × 0.18
Space group	$P\bar{1}$
T/°C	20
a/Å	11.706(4)
b/Å	11.889(5)
c/Å	13.080(3)
α/°	114.10(3)
β/°	104.76(4)
γ/°	90.85(3)
U/Å^3	1592.23
λ(Mo-Kα)/Å	0.7107
Z	1
D_c/g cm^{-3}	1.658
μ(Mo-Kα)/cm^{-1}	18.44
F(000)	818
Absorption corrections	0.902–1.097
Total no. of reflections	4432
No. of obs. reflections [$I > 3\sigma(I)$]	2622
$R(F_o)$[a]	0.047
R'[b]	0.047

[a] $R = \Sigma(|F_o| - |F_c|)/\Sigma(F_o)$. [b] $R' = [\Sigma w(F_o - F_c)^2/w(F_o)^2]^{\frac{1}{2}}$.

Table 2 Final positional (× 10^4) parameters for $[Fe_6(\mu_3\text{-}S)_8(PEt_3)_6][PF_6]_2$ **2**

Atom	x	y	z
Fe(1)	4 528(1)	1 121(1)	1 240(1)
Fe(2)	6 330(1)	1 110(1)	402(1)
Fe(3)	4 160(1)	678(1)	−954(1)
S(1)	5 025(2)	2 480(2)	580(2)
S(2)	4 173(2)	−577(2)	1 535(2)
S(3)	6 445(2)	1 315(2)	2 211(2)
S(4)	2 750(2)	582(2)	−96(2)
P(1)	3 898(2)	2 528(2)	2 724(2)
P(2)	7 934(2)	2 573(2)	980(2)
P(3)	3 024(2)	1 432(3)	−2 167(2)
P(4)	8 840(5)	3 122(5)	6 236(6)
F(1)	8 927(11)	4 531(12)	6 803(11)
F(2)	10 176(13)	3 215(13)	6 397(12)
F(3)	8 813(15)	1 725(16)	5 818(15)
F(4)	7 516(23)	3 102(22)	6 460(21)
F(5)	9 206(17)	3 180(17)	7 554(17)
F(6)	8 120(19)	2 862(20)	5 091(20)
C(1)	3 720(10)	4 014(10)	2 663(10)
C(2)	2 787(11)	3 984(12)	1 616(11)
C(3)	2 461(9)	1 982(10)	2 786(9)
C(4)	1 946(11)	2 901(11)	3 705(10)
C(5)	4 881(10)	2 985(10)	4 192(10)
C(6)	4 990(12)	1 958(12)	4 582(13)
C(7)	8 447(10)	3 589(10)	2 536(10)
C(8)	7 573(12)	4 391(12)	3 033(12)
C(9)	9 283(10)	1 952(10)	740(10)
C(10)	9 262(12)	1 252(13)	−531(11)
C(11)	7 683(9)	3 572(10)	221(10)
C(12)	8 738(11)	4 507(12)	489(12)
C(13)	3 400(9)	3 097(10)	−1 707(10)
C(14)	4 591(11)	3 470(12)	−1 801(12)
C(15)	3 092(10)	691(10)	−3 659(9)
C(16)	2 291(11)	1 113(12)	−4 502(11)
C(17)	1 444(9)	1 323(10)	−2 283(10)
C(18)	781(11)	14(11)	−2 852(11)

This same procedure was adopted in all the previous calculations.[1] Relevant interatomic distances for the model compound $[Fe_6(\mu_3\text{-}S)_8(PH_3)_6]^{n+}$ are: Fe–Fe 2.62, Fe–S 2.25, Fe–P 2.30 Å, which correspond to the average values observed in the crystal structure of complex **2**. The model molecule and the reference system are shown in Fig. 1.

The calculations were performed using the standard version of the Xα-SW method as implemented in the COOK5/TAMU1 program written by M. Cook, B. Bursten and G. Stanley. The molecular properties were calculated according to the procedures described by Case, Cook and Karplus.[24–26]

The actual coordinates used in the calculations were the same as those previously reported[1] for $[Fe_6(\mu_3\text{-}S)_8(PH_3)_6]^+$. The parameters used are given in Table 3. The α values used for Fe, S and P were those tabulated by Schwartz[27] for the free atoms. For H we used the spin-polarised α value suggested by Slater.[28a] The α values for the inter- and outer-sphere regions were determined by averaging the atomic values, weighted by the number of atomic valence electrons. Core levels were assumed to be confined in the atomic spheres and included in the SCF procedure. The sphere radii were computed using the Norman[28b] procedure and reduced by a constant factor, $R = 0.88$, to avoid excessive overlap between the atomic spheres. A radius of 0.5292 Å was assigned to the hydrogen atoms as commonly done in the literature.[1,6,15]

One-electron energy levels were computed for $n = 0$ using spin-restricted calculations and filling up the levels with electrons in order of increasing energy. Spin-unrestricted calculations were performed subsequently and the occupation of the one-electron energy levels was then changed in order to reach the maximum M_S state compatible with the charge of the molecule. The relative stabilities of the various oxidation states of the cluster were investigated by comparing the total energies and the Hellmann–Feynman forces[29] computed on the iron atoms. In a fixed arrangement of nuclei, this force is the sum of the electrostatic forces exerted by the nuclei other than the nucleus under examination and by an electron cloud whose charge density is $-e\rho(r)$, $\rho(r)$ being the electron density computed after the SCF procedure. Relative variations of the Hellmann–Feynman force have recently been applied to rationalise structural features in clusters.[6,15]

In Table 4 the one-electron energies and distribution of charges computed for $[Fe_6(\mu_3\text{-}S)_8(PH_3)_6]^+$ using spin-polarised calculations are reported. The total number of unpaired electrons is seven corresponding to a $S = \frac{7}{2}$ state.

The calculations were performed in IBM-RISC/6000 and DECpc-αXP computers.

Table 3 Atomic parameters used in the Xα-SW calculations for the model cluster $[Fe_6(\mu_3\text{-}S)_8(PH_3)_6]^+$

Atom	l_{max}	α	Sphere radius/Å
Out	3	0.727 20	5.461 9
Fe	2	0.711 51	1.204 9
P	1	0.726 20	1.300 7
S	1	0.724 75	1.283 2
S′	1	0.724 75	1.283 2
H(1)	0	0.777 25	0.529 2
H(2)	0	0.777 25	0.529 2

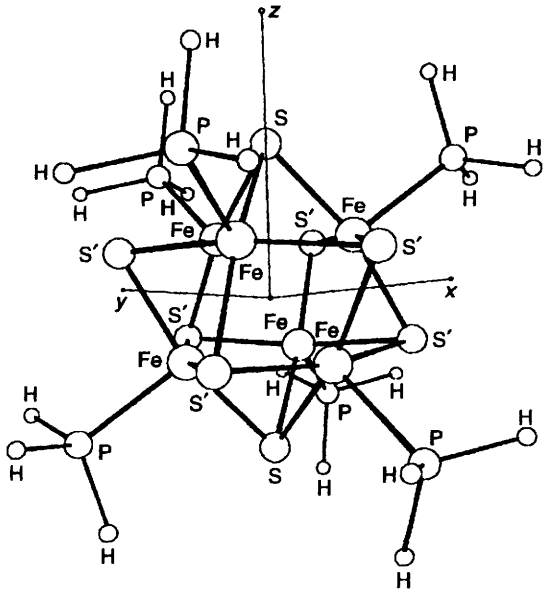

Fig. 1 The model cation $[Fe_6(\mu_3\text{-}S)_8(PH_3)_6]^{n+}$ used in the Xα-SW calculations and the reference frame employed

Results and Discussion

Description of the Structure.—The molecular structure of complex **2** consists of discrete $[Fe_6(\mu_3\text{-}S)_8(PEt_3)_6]^{2+}$ cluster cations and hexafluorophosphate anions. Fig. 2 shows a perspective view of the cluster cation, and selected bond distances and angles are given in Table 5. The cation possesses C_i symmetry and is isostructural with all the members of the series $[M_6S_8(PEt_3)_6]^{n+}$ (M = Fe, $n = 1$ or 2; M = Co, $n = 0$ or 1),[6,8,14] being built up of an octahedral cluster of iron with all the faces capped by triply bridging sulfur atoms. Moreover each metal atom is linked to a triethylphosphine group. An inspection of Table 2 shows that the bond distances and angles match quite closely with those required by an idealised S_6 symmetry. The bond distances and angles are equal, within the standard deviations, to those observed in the corresponding tetraphenylborate salt.

Magnetic Measurements.—The measured temperature dependence of the magnetic susceptibility for $[Fe_6(\mu_3\text{-}S)_8(PEt_3)_6][PF_6]$ **1** is shown in Fig. 3(*a*). The effective magnetic moment, $\mu_{eff} = \sqrt{8\chi T}$, is nearly constant in the temperature range 300–20 K at 7.7 μ_B. This is typical Curie–Weiss paramagnetic behaviour and the observed value of μ_{eff} compares well with the spin only (SO) value for $S = \frac{7}{2}$, $\mu_{SO} = 7.9\ \mu_B$, computed with $g = 2.00$. The low-temperature magnetisation of **1** as a function of the applied magnetic field, B, is shown in Fig. 3(*b*) in the form m *vs.* $B\,T^{-1}$, where m is the average magnetic moment per ion. The experimental data were taken at 2.3, 4.3 and 9.4 K. The points approach a saturation value, the value of m measured at 2.3 K and 7.0 T being 7.0 μ_B.

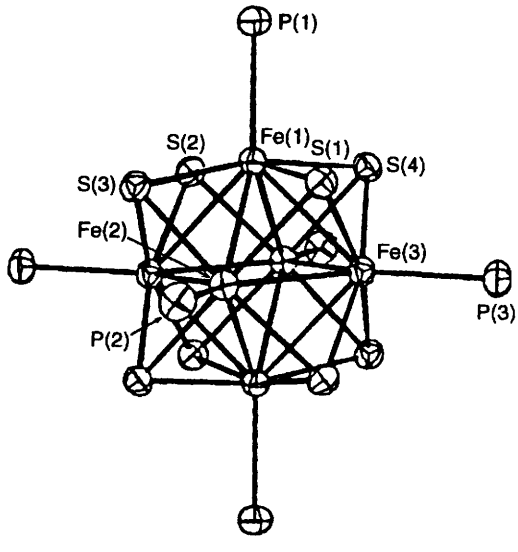

Fig. 2 Perspective view of the cluster cation $[Fe_6(\mu_3\text{-}S)_8(PEt_3)_6]^{2+}$ in the hexafluorophosphate salt

Table 4 Valence energy levels and percent charge distribution for $[Fe_6(\mu_3\text{-}S)_8(PH_3)_6]^+$ computed with spin-unrestricted Xα-SW calculations*

Level	Energy/eV	Fe	P	S	S′	H(1)	H(2)	Int	Out
$11A_{2u}\downarrow$	−5.691	54	0	7	22	0	0	15	2
$11A_{2u}\uparrow$	−6.525	48	0	9	28	0	0	13	1
$14E_g\downarrow$	−6.588	55	0	5	24	0	0	16	1
$11A_{1g}\downarrow$	−6.595	55	0	12	17	0	0	16	1
$14E_u\downarrow$	−6.941	53	0	9	26	0	0	12	0
$13E_g\downarrow$	−7.162	59	13	3	10	1	1	11	2
$10A_{2u}\downarrow$	−7.350	61	14	1	12	0	1	9	2
$13E_u\downarrow$	−7.381	61	13	4	8	1	1	9	2
$14E_g\uparrow$	−7.394	46	0	7	31	0	0	15	0
$11A_{1g}\uparrow$	−7.401	46	0	15	23	0	0	15	0
$14E_u\uparrow$	−7.688	41	0	12	34	0	0	13	0
$13E_g\uparrow$	−7.990	47	19	4	13	1	2	12	2
$10A_{2u}\uparrow$	−8.168	46	20	0	19	1	1	11	2
$13E_u\uparrow$	−8.201	46	20	7	11	2	1	11	2
$12E_u\downarrow$	−8.669	85	0	4	7	0	0	4	0
$4A_{1u}\downarrow$	−8.671	85	0	0	11	0	0	4	0
$4A_{2g}\downarrow$	−8.829	81	0	0	15	0	0	4	0
$12E_g\downarrow$	−8.831	81	0	5	9	0	0	4	0
$3A_{2g}\downarrow$	−9.156	97	0	0	0	0	0	3	0
$11E_u\downarrow$	−9.451	63	3	2	18	0	1	12	0
$9A_{2u}\downarrow$	−9.460	63	3	11	10	1	0	12	0
$11E_g\downarrow$	−9.642	89	0	1	3	0	0	6	0
$4A_{2g}\uparrow$	−9.771	37	0	0	54	0	0	9	0
$12E_g\uparrow$	−9.777	37	0	20	33	0	0	9	0
$10A_{1g}\downarrow$	−9.798	48	24	0	1	0	2	23	0
$10E_g\downarrow$	−9.838	77	0	1	10	0	0	10	0
$9A_{1g}\downarrow$	−9.866	78	1	7	4	1	0	10	0
$4A_{1u}\uparrow$	−9.889	73	0	0	21	0	0	6	0
$12E_u\uparrow$	−9.892	73	0	8	13	0	0	6	0
$3A_{1u}\downarrow$	−9.922	86	1	0	4	0	1	8	0
$10E_u\downarrow$	−9.924	86	1	1	2	1	1	8	0
$11E_u\uparrow$	−10.240	47	1	4	33	0	1	13	0
$9A_{2u}\uparrow$	−10.249	47	1	19	18	1	0	13	0
$10A_{1g}\uparrow$	−10.298	36	36	0	1	1	2	23	1
$2A_{2g}\downarrow$	−10.390	16	2	0	63	0	2	16	0
$9E_g\downarrow$	−10.399	16	2	24	39	1	1	16	0
$3A_{2g}\uparrow$	−10.620	97	0	0	0	0	0	3	0
$11E_g\uparrow$	−10.835	58	2	10	15	1	1	12	0
$2A_{2g}\uparrow$	−10.853	57	3	0	23	0	3	11	0
$10E_g\uparrow$	−10.866	59	2	2	22	0	2	12	0
$9A_{1g}\uparrow$	−10.890	60	1	12	12	1	0	13	0
$9E_g\uparrow$	−10.926	85	2	2	4	0	0	7	0
$3A_{1u}\uparrow$	−11.131	78	4	0	6	0	3	9	0
$10E_u\uparrow$	−11.143	79	4	2	4	1	1	9	0
$8A_{2u}\downarrow$	−11.268	35	0	6	45	0	0	14	0
$9E_u\downarrow$	−11.275	35	0	16	35	0	0	14	0
$9E_u\uparrow$	−11.785	42	6	12	24	0	1	15	0
$8A_{2u}\uparrow$	−11.788	43	6	3	33	0	0	15	0
$8E_u\downarrow$	−12.193	44	1	15	31	0	0	8	0
$8E_g\downarrow$	−12.216	33	45	1	2	1	3	13	2
$7E_g\downarrow$	−12.300	23	4	17	38	0	1	15	0
$2A_{1u}\downarrow$	−12.313	20	14	0	39	0	7	20	0
$8A_{1g}\downarrow$	−12.343	22	2	7	51	1	0	16	0
$7E_u\downarrow$	−12.380	20	14	11	27	4	2	20	0
$6E_u\downarrow$	−12.387	26	45	0	6	1	4	15	2
$7A_{2u}\downarrow$	−12.389	27	46	3	2	1	3	15	2
$2A_{1u}\uparrow$	−12.628	36	16	0	23	0	7	17	0
$8E_g\uparrow$	−12.643	42	40	0	0	1	3	12	2
$7E_g\uparrow$	−12.669	42	3	13	29	0	1	12	0
$8E_u\uparrow$	−12.677	35	16	11	12	4	3	18	0
$8A_{1g}\uparrow$	−12.688	40	0	8	40	0	0	13	0
$7A_{1g}\downarrow$	−12.730	24	18	26	9	5	2	16	0
$6E_g\downarrow$	−12.763	24	15	0	38	1	6	16	0
$7E_u\uparrow$	−12.777	43	38	0	0	2	3	12	2
$7A_{2u}\uparrow$	−12.778	43	38	0	0	0	4	12	2
$6A_{1g}\downarrow$	−12.801	41	36	0	4	1	3	15	1
$6E_u\uparrow$	−12.888	57	1	6	29	0	0	7	0
$7A_{1g}\uparrow$	−12.931	14	34	10	4	10	5	22	1
$6E_g\uparrow$	−12.973	14	31	0	19	2	12	23	0
$6A_{2u}\downarrow$	−12.994	22	18	22	14	4	3	16	0
$6A_{2u}\uparrow$	−13.018	6	39	9	3	12	5	26	0
$5E_u\uparrow$	−13.031	7	39	0	12	2	14	26	1

Table 4 (*continued*)

Level	Energy/eV	Fe	P	S	S'	H(1)	H(2)	Int	Out
$5E_u\downarrow$	−13.041	5	38	1	15	3	13	25	0
$5A_{2u}\downarrow$	−13.071	18	20	0	33	5	4	19	0
$1A_{2g}\uparrow$	−13.383	4	44	0	3	0	18	31	0
$5E_g\uparrow$	−13.383	4	44	1	2	9	9	31	0
$6A_{1g}\uparrow$	−13.395	55	24	1	4	1	2	12	0
$5E_g\downarrow$	−13.401	2	45	1	2	9	9	32	0
$1A_{2g}\downarrow$	−13.402	2	45	0	2	0	18	32	0
$5A_{2u}\uparrow$	−13.536	43	0	10	38	0	0	9	0
$5A_{1g}\downarrow$	−13.596	18	28	7	11	7	4	24	1
$4E_u\downarrow$	−13.606	6	34	7	10	7	6	30	0
$4E_g\downarrow$	−13.617	17	29	4	13	2	9	25	1
$1A_{1u}\downarrow$	−13.623	6	33	0	17	0	13	30	1
$4E_u\uparrow$	−13.649	11	28	8	12	6	5	28	1
$1A_{1u}\uparrow$	−13.669	11	28	0	21	0	11	28	1
$3E_u\downarrow$	−13.899	22	12	4	37	0	4	20	0
$4A_{2u}\downarrow$	−13.910	22	12	24	17	3	1	20	0
$5A_{1g}\uparrow$	−13.931	39	12	12	15	3	1	17	0
$4E_g\uparrow$	−13.938	39	13	4	22	1	4	17	0
$4A_{1g}\downarrow$	−13.945	20	1	15	44	0	0	19	0
$3E_g\downarrow$	−13.970	25	6	12	36	0	1	21	0
$4A_{1g}\uparrow$	−14.055	21	1	16	41	0	0	20	0
$3E_u\uparrow$	−14.147	31	8	4	37	0	2	18	0
$4A_{2u}\uparrow$	−14.156	31	8	25	16	2	0	18	0
$3E_g\uparrow$	−14.262	34	3	11	33	0	0	18	0

* Core levels and diffuse Rydberg orbitals are not shown.

The curve computed using the Brillouin function (1), where $y = g\,\mu_B\,S/kT$, with $g = 2.0$ and $S = \frac{7}{2}$, is shown in Fig. 3(*b*) as the solid line. These data indicate that for cluster **1** a $S = \frac{7}{2}$ state is populated over the whole temperature range and excited spin states or inter-cluster magnetic interactions do not contribute appreciably to the value of the magnetisation.

$$m = g\,\mu_B\,S\left[\frac{2S+1}{2S}\coth\left(\frac{2S+1}{2S}y\right) - \frac{1}{2S}\coth\left(\frac{y}{2S}\right)\right] \quad (1)$$

The measured temperature dependence of the magnetic susceptibility for $[Fe_6(\mu_3\text{-}S)_8(PEt_3)_6][PF_6]_2$ **2**, in the form χT *vs.* T, is shown in Fig. 4(*a*). The observed effective magnetic moment decreases on decreasing temperature from a value of 5.5 emu mol^{-1} K ($\mu_{eff} = 6.6\ \mu_B$) at 290 K to 2.3 emu mol^{-1} K ($\mu_{eff} = 4.3\ \mu_B$) at 4.2 K. Below ≈20 K it remains almost constant forming a plateau at $\mu_{eff} \approx 4.3\ \mu_B$. Assigning a 2− charge to the sulfur atoms, the formal charge on the metal centres is 3+. Each iron(III) centre, therefore, possesses from one to five unpaired electrons according to its spin state (low-spin: $S = \frac{1}{2}$; high-spin: $S = \frac{5}{2}$; intermediate spin: $S = \frac{3}{2}$). Since χT decreases with temperature low lying excited magnetic states should be near to the ground state, which, however, is magnetic, since the magnetic moment at 4.2 K is still different from zero. The room-temperature value of μ_{eff} is distinctly higher than expected for six non-interacting low-spin iron(III) ions ($\mu_{eff} = 4.24\ \mu_B$ for $g = 2.0$). It is also distinctly lower than the values expected for six $S = \frac{3}{2}$ and six $S = \frac{5}{2}$ spins, which are 9.5 and 14.5 μ_B respectively, indicating that some coupling is operating between the iron(III) centres. On the other hand, the value observed at 4.2 K corresponds well with six non-interacting low-spin iron(III) ions.

It is general practice to rationalise the magnetic properties of transition-metal clusters using the isotropic Heisenberg–Dirac–van Vleck spin Hamiltonian. In this formalism the electron–electron interactions are reduced to an effective magnetic coupling between the total spins of the interacting centres, equation (2). The eigenvalues of (2), $E(S)$, can conveniently

$$\mathscr{H}_S = \sum_{i<j} J_{ij}\boldsymbol{S}_i\cdot\boldsymbol{S}_j \quad (2)$$

be computed[10] in the spin space (S_{12}, S_{34}, S_{56}, S^*, S), where $S_{ij}(S_{ij}+1)$ is the eigenvalue of $\boldsymbol{S}_{ij}^2$ ($\boldsymbol{S}_{ij} = \boldsymbol{S}_i + \boldsymbol{S}_j$); $S^*(S^*+1)$ is the eigenvalue of $\boldsymbol{S}^{*2}$ ($\boldsymbol{S}^* = \boldsymbol{S}_{34} + \boldsymbol{S}_{56}$); and $S(S+1)$ is the eigenvalue of the total spin operator $\boldsymbol{S}^2$ ($\boldsymbol{S} = \boldsymbol{S}^* + \boldsymbol{S}_{12}$).

Magnetic susceptibility can be computed using the van Vleck equation (3). Using the J_{ij} constants in equation (2) as

$$\chi = \frac{N\mu_B^2 g^2 \sum S(S+1)(2S+1)e^{-E(S)/kT}}{3kT\sum(2S+1)e^{-E(S)/kT}} \quad (3)$$

parameters, (3) can be fitted to experimental data by minimising the agreement function (4) using a Simplex minimisation routine.

$$F^2 = \sum(\chi_{obs} - \chi_{calc})^2 \quad (4)$$

The Hamiltonian (2) has been successfully applied to the description of the magnetic properties of low- and high-nuclearity transition-metal clusters. The physical basis[30] of the spin Hamiltonian (2) is a Heitler–London picture of the bonding in which the interacting spins are localised onto the so-called magnetic centres and the exchange interactions are generally referred to as weak-bonding interactions.

The results of the fitting are shown in Fig. 4(*a*) and 4(*b*) as solid lines. The model used in the fitting procedure will be discussed later.

The measured field dependence of the average magnetic moment per ion at 2.3, 4.3 and 9.4 K is shown in Fig. 4(*c*) for magnetic field values in the range 0.02–7.0 T. It is apparent that the data deviate significantly from the paramagnetic behaviour described by a Brillouin function and at 2.3 K the saturation value is not yet reached at 7.0 T. This is indicative of the presence of excited magnetic states close to the ground state still at 2.3 K. Since complex **2** is a non-Kramers ion these states can originate from the exchange interaction (2) as well as from anisotropic exchange and/or magnetic interactions.[10] Also inter-cluster magnetic interactions can be effective.

Mössbauer Spectra.—The Mössbauer spectra of complex **1** recorded on polycrystalline samples are shown in Fig. 5 and the relevant parameters reported in Table 6.

The 80 K spectrum is characterised by a narrow quadrupole

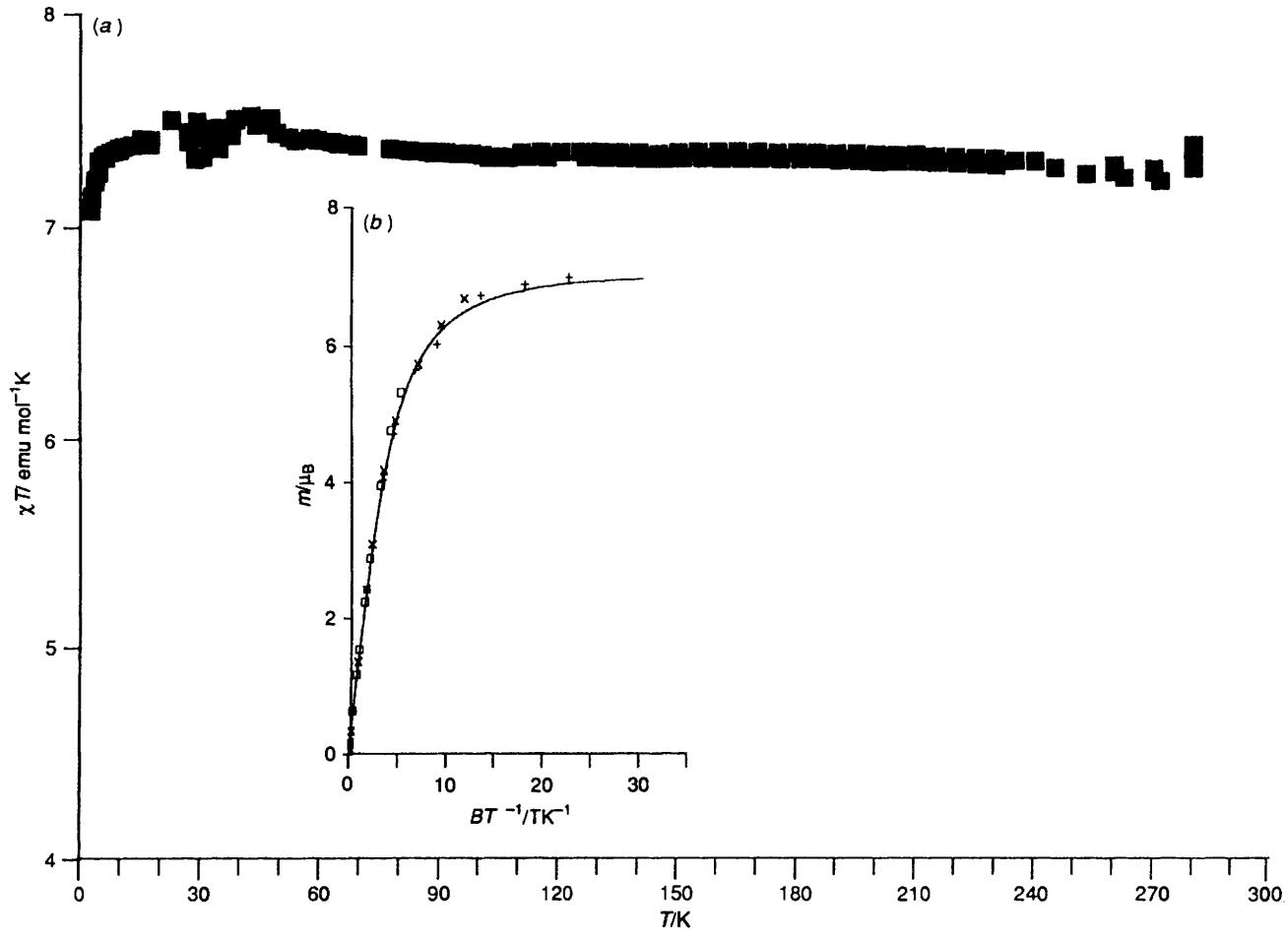

Fig. 3 Magnetic data for $[Fe_6(\mu_3\text{-}S)_8(PEt_3)_6][PF_6]$ **1**. (*a*) Temperature dependence of the magnetic susceptibility in the form χT *vs.* *T*. (*b*) Field dependence of the magnetization in the form *m vs.* BT^{-1} at 2.3 (+), 4.3 (×) and 9.4 K (□). The solid line represents the computed curve (see text)

split doublet only, with parameters in the range usually observed for iron(III) complexes in the low-spin state. The observation of low-spin iron(III) at this temperature is in agreement with the magnetic data which show that, down to 20 K, the cluster has a $S = \frac{7}{2}$ ground state that can be described as being due to a ferromagnetic interaction between five low-spin iron(III) ions ($S = \frac{1}{2}$) and one iron(II) ion in the $S = 1$ intermediate-spin state. However, no evidence for the iron(II) ion in an intermediate-spin state is observable in the Mössbauer spectrum. The signal coming from such a species can be hidden under the strong iron(III) signal, or, more likely and consistent with the observed crystallographic equivalence of the iron atoms, the extra electron is delocalised over the six iron ions and the spectrum is due to the weighted average of the two components.

Below 80 K, a broad hyperfine structure appears in zero applied field, that sharpens slowly on lowering the temperature, until, at ≈5.0 K, a six line pattern develops. During the whole process the central doublet remains perfectly sharp: its linewidth decreases from 0.50 to 0.36 mm s^{-1}. The origin of a hyperfine sextet can be of various kinds. First, the exact condition for the appearance of the magnetic splitting is $\tau_R \gg \tau_L \approx 10^{-8}$ s, if $\tau_N \gg \tau_L$, where τ_N is the lifetime of the nuclear excited state and τ_L is the Larmor time of the ground level. Therefore, a paramagnetic species shows a hyperfine split spectrum when the electronic relaxation time, τ_R, is sufficiently long (slow paramagnetic relaxation).[31] In the fast relaxation regime ($\tau_R \ll \tau_L$) it shows a doublet. Secondly, the internal hyperfine fields responsible for the magnetic splitting are found in a magnetically ordered state with long-range correlation between the magnetic centres or can arise from anisotropic exchange and/or magnetic interactions which set up the preferred orientation of the magnetic moments in the solid. Since the low-temperature magnetisation of complex **1** does not show the existence of any particular interaction between the clusters or any relevant effect of anisotropic interaction, we rule out the latter explanation and assign the 5.0 K spectrum of Fig. 5(*a*) to a slow paramagnetic relaxation. Each of the four Kramers doublets which form the $S = \frac{7}{2}$ ground spin state gives rise to a Mössbauer spectrum and, depending on their relaxation rates, a paramagnetic doublet or a magnetic six line pattern may be obtained. The resulting Mössbauer spectrum is a superposition of the four subspectra weighted by the relative Boltzmann population of each state. If only one of the doublets, probably the $M_S = \pm\frac{7}{2}$, relaxes slowly, a spectrum showing a doublet and a sextet may be obtained.

The Mössbauer spectrum of the dipositive cluster in the tetraphenylborate salt has been recorded previously.[32] It is characterised by a narrow quadrupole split doublet over the temperature range investigated. The small value of the linewidth, about 0.26 mm s^{-1}, is indicative of the electronic and crystallographic equivalence of the six iron ions in the cluster. The temperature dependences of the isomer and quadrupole shifts have been discussed.

Electronic Structure.—The one-electron energy levels computed for $[Fe_6(\mu_3\text{-}S)_8(PH_3)_6]^+$, as a model molecule for **1**, using spin-unrestricted calculations are shown in Table 4, together with the partitioning of the electron density into the atomic, inter-atomic and outer-atomic regions. In order to assign the bonding character of the molecular orbitals it is, however, convenient to look at the spin-restricted results. These are presented graphically in Fig. 6 as density of states (DOS) plots. The DOS profile was obtained using a Gaussian distribution

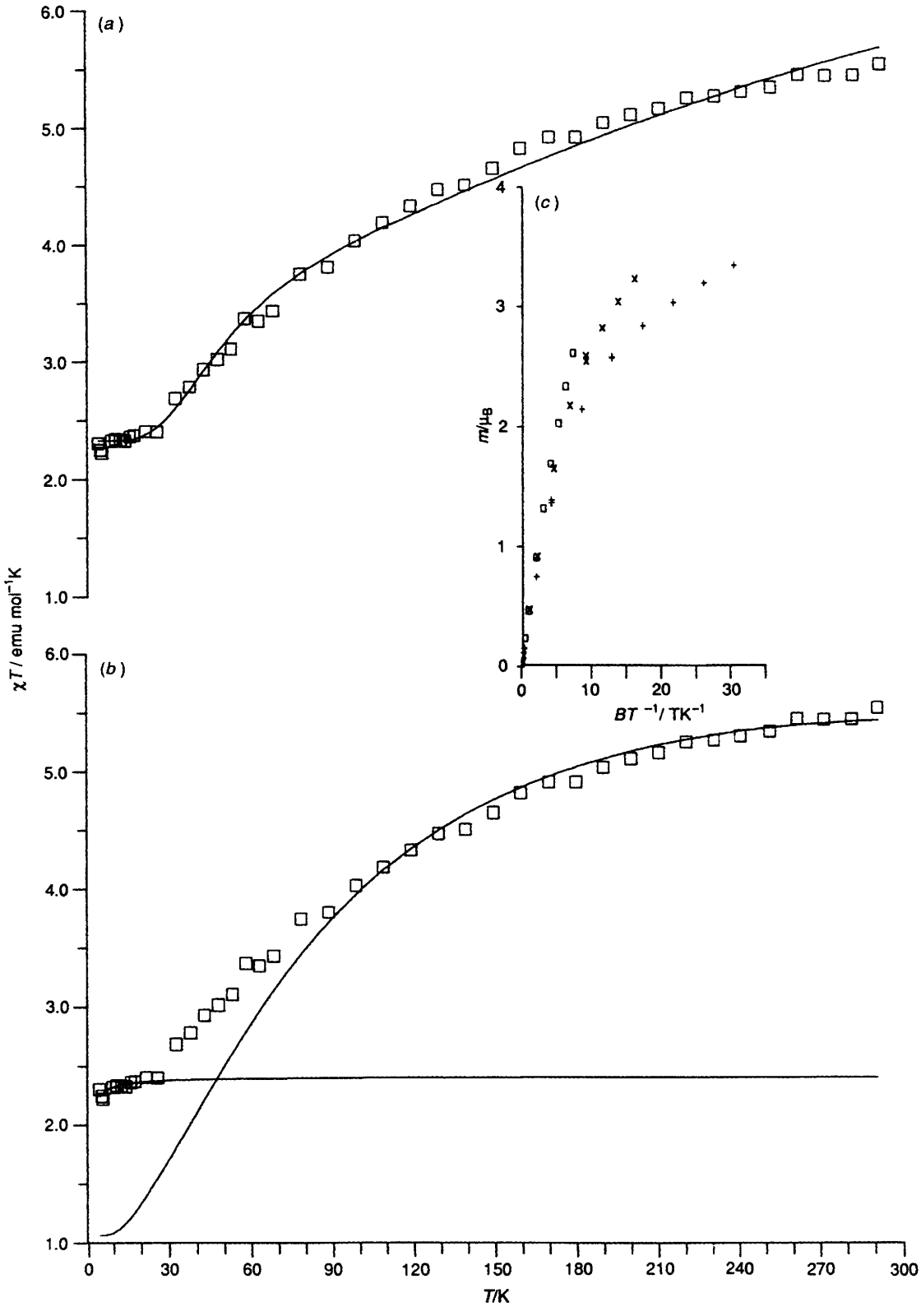

Fig. 4 Magnetic data for $[Fe_6(\mu_3\text{-}S)_8(PEt_3)_6][PF_6]_2$ **2**. (*a*), (*b*) Temperature dependence of the magnetic susceptibility in the form χT *vs.* T; the solid lines represent the best fit results (see text). (*c*) Field dependence of the magnetization in the form m *vs.* BT^{-1} at 2.3 (+), 4.3 (×) and 9.4 K (□)

function $N(E)$ around the ith eigenvalue ε_i [equation (5)], where the linewidth of the distribution $\sigma = 0.20$ eV was used.

$$N(E) = \frac{\sum_i p_i e^{-(E-\varepsilon_i)^2/2\sigma^2}}{\sqrt{2\pi\sigma}} \quad (5)$$

The p_i values are the weights assigned to each particular level. Putting $p_i = 1$ we obtain the total DOS, putting p_i equal to the gross atomic population obtained from the SW calculations we have computed the partial DOS figures. These figures represent the overall contribution of one atomic centre to the energy level bands. The electronic populations which are left out of Fig. 6

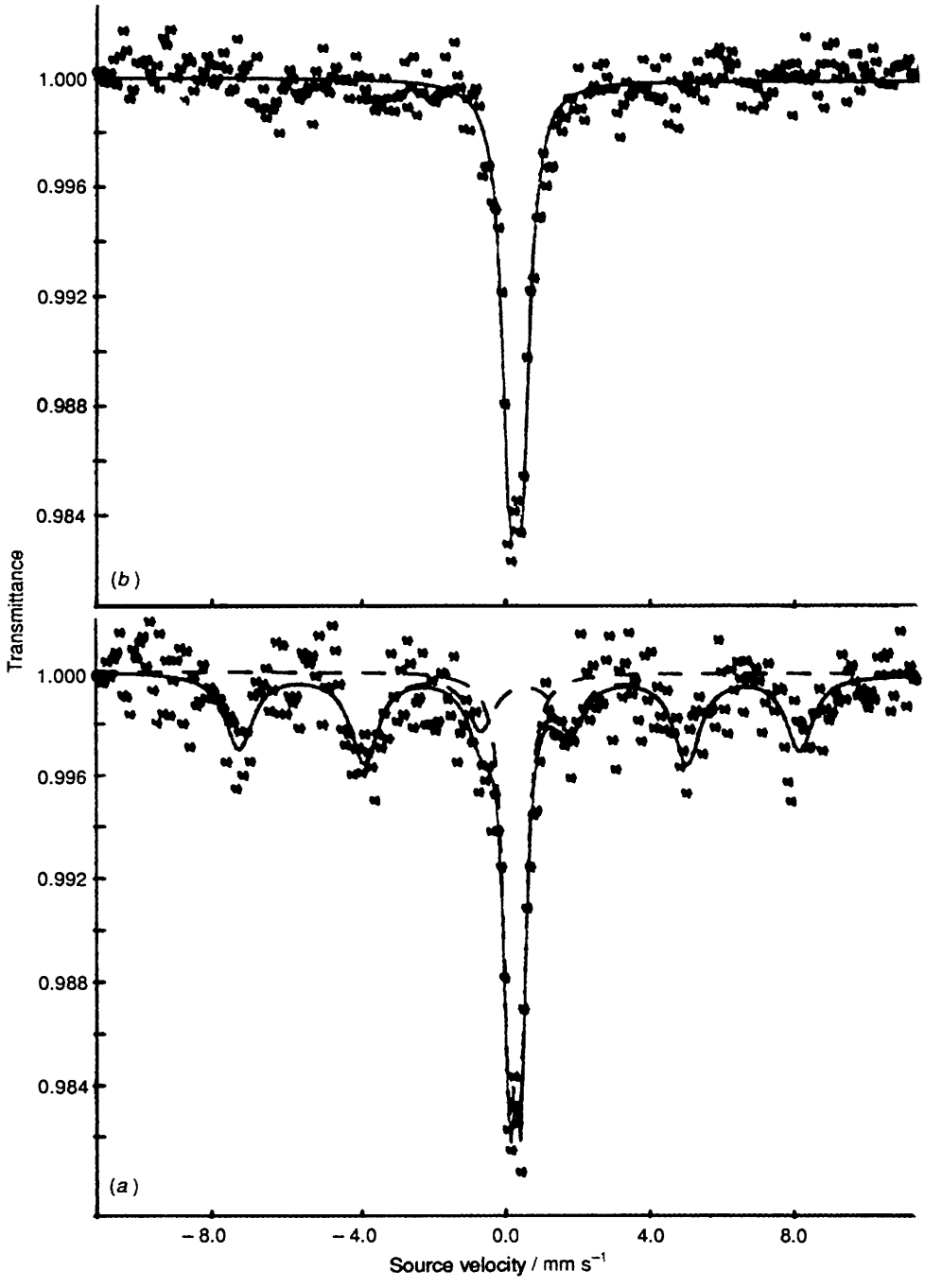

Fig. 5 Mössbauer spectra of $[Fe_6(\mu_3\text{-}S)_8(PEt_3)_6][PF_6]$ **1** at (*a*) 5.0 and (*b*) 80 K

represent the hydrogen contribution and the inter- and outer-sphere charges.

Apart from a general shift of the energy levels towards higher energies, caused by the smaller positive charge, the relative ordering of the energy levels closely follows that computed for the doubly charged species.[1] The nature of the molecular orbitals (MOs) can be read from the partitioning of the electronic density in the atomic and extra-atomic regions. Non-bonding orbitals have, in fact, charges well localised in the atomic spheres, while bonding and anti-bonding orbitals show charges distributed into several atomic spheres and also generally spread out into the inter-sphere region. Almost non-bonding S (3s) orbitals lie between −23.0 and −21.6 eV; between −20.3 and −20.2 eV there are the six MOs formed by the 3s orbitals of P and 1s orbitals of H. Bonding iron–sulfur–phosphorus orbitals form a series of closely spaced levels between −14.1 and −12.4 eV; at −11.5 eV lie the $8A_{2u}$ and $9E_u$ orbitals which can be assigned as bonding iron–sulfur with negligible contribution from phosphorus. This energy difference suggests that phosphorus atoms make a substantial contribution to the stabilisation of the cluster. Anti-bonding and almost non-bonding Fe 3d orbitals form a band which starts from −10.5 eV and extends to −5 eV. An energy gap of ≈1.4 eV lies above the Fermi level, $12E_u + 4A_{1u}$, at −9.2 eV. The unoccupied levels above the Fermi level have a sizeable contribution from both P and S atoms while the Fe–P anti-bonding levels at −10.03 eV have negligible contribution from sulfur atoms. This difference in composition can be responsible for the energy gap inside the anti-bonding d band.

The presence of this energy gap governs the magnetic and chemical properties of the whole cluster. In fact this poses a limit to the possible spin configurations which can arise from the

Table 5 Selected bond distances (Å) and angles (°) for $[Fe_6(\mu_3\text{-}S)_8(PEt_3)_6][PF_6]_2$ **2**

Fe(1)–Fe(2)	2.611(2)	Fe(1)–Fe(3′)	2.609(2)
Fe(1)–Fe(3)	2.613(2)	Fe(2)–Fe(3)	2.605(2)
Fe(1)–Fe(2′)	2.613(2)	Fe(2)–Fe(3′)	2.607(1)
Fe–Fe (mean)	2.610(1)		
Fe(1)–S(1)	2.250(3)	Fe(2)–S(3)	2.245(3)
Fe(1)–S(2)	2.255(3)	Fe(2)–S(4′)	2.235(3)
Fe(1)–S(3)	2.235(3)	Fe(3)–S(1)	2.243(2)
Fe(1)–S(4)	2.234(2)	Fe(3)–S(2′)	2.255(3)
Fe(2)–S(1)	2.233(3)	Fe(3)–S(3′)	2.234(2)
Fe(2)–S(2′)	2.256(3)	Fe(3)–S(4)	2.245(3)
Fe–S (mean)	2.243(3)		
Fe(1)–P(1)	2.286(3)	Fe(3)–P(3)	2.283(3)
Fe(2)–P(2)	2.287(3)		
Fe–P (mean)	2.285(1)		
Fe(2)–Fe(1)–Fe(3)	59.81(5)	S(2′)–Fe(2)–P(2)	98.59(12)
Fe(2)–Fe(1)–Fe(2′)	89.76(6)	S(4′)–Fe(2)–P(2)	99.72(10)
Fe(2)–Fe(1)–Fe(3′)	59.93(6)	Fe(1)–Fe(3)–Fe(2)	60.05(5)
Fe(3)–Fe(1)–Fe(2′)	59.84(6)	Fe(1)–Fe(3)–Fe(1′)	90.26(7)
Fe(3)–Fe(1)–Fe(3′)	89.74(6)	Fe(1)–Fe(3)–Fe(2′)	60.06(6)
Fe(2′)–Fe(1)–Fe(3′)	59.84(5)	Fe(2)–Fe(3)–Fe(1′)	60.15(5)
S(1)–Fe(1)–S(2)	165.96(11)	Fe(2)–Fe(3)–Fe(2′)	90.03(7)
S(1)–Fe(1)–S(3)	89.14(11)	Fe(1′)–Fe(3)–Fe(2′)	60.08(6)
S(1)–Fe(1)–S(4)	89.44(11)	S(1)–Fe(3)–S(2′)	88.94(10)
S(1)–Fe(1)–P(1)	96.02(12)	S(1)–Fe(3)–S(3′)	166.22(13)
S(2)–Fe(1)–S(3)	89.03(11)	S(1)–Fe(3)–S(4)	89.33(10)
S(2)–Fe(1)–S(4)	88.93(11)	S(1)–Fe(3)–P(3)	99.41(11)
S(2)–Fe(1)–P(1)	98.02(13)	S(2′)–Fe(3)–S(3′)	89.08(10)
S(3)–Fe(1)–S(4)	165.81(11)	S(2′)–Fe(3)–S(4)	166.22(13)
S(3)–Fe(1)–P(1)	98.78(9)	S(2′)–Fe(3)–P(3)	98.89(13)
S(4)–Fe(1)–P(1)	95.41(10)	S(3′)–Fe(3)–S(4)	89.36(10)
Fe(1)–Fe(2)–Fe(3)	60.15(5)	S(3′)–Fe(3)–P(3)	94.37(10)
Fe(1)–Fe(2)–Fe(1′)	90.24(6)	S(4)–Fe(3)–P(3)	94.89(12)
Fe(1)–Fe(2)–Fe(3′)	60.00(6)	Fe(1)–S(1)–Fe(2)	71.25(10)
Fe(3)–Fe(2)–Fe(1′)	60.00(5)	Fe(1)–S(1)–Fe(3)	71.14(9)
Fe(3)–Fe(2)–Fe(3′)	89.97(6)	Fe(2)–S(1)–Fe(3)	71.18(8)
Fe(1′)–Fe(2)–Fe(3′)	60.09(6)	Fe(1)–S(2)–Fe(2′)	70.78(11)
S(1)–Fe(2)–S(3)	89.34(11)	Fe(1)–S(2)–Fe(3′)	70.68(11)
S(1)–Fe(2)–S(2′)	89.17(11)	Fe(2′)–S(2)–Fe(3′)	70.54(10)
S(1)–Fe(2)–S(4′)	166.34(11)	Fe(1)–S(3)–Fe(2)	71.29(9)
S(1)–Fe(2)–P(2)	93.94(10)	Fe(1)–S(3)–Fe(3′)	71.42(7)
S(3)–Fe(2)–S(2′)	166.28(11)	Fe(2)–S(3)–Fe(3′)	71.18(9)
S(3)–Fe(2)–S(4′)	89.35(11)	Fe(1)–S(4)–Fe(3)	71.41(9)
S(3)–Fe(2)–P(2)	95.12(11)	Fe(1)–S(4)–Fe(2′)	71.57(9)
S(2′)–Fe(2)–S(4′)	88.89(11)	Fe(3)–S(4)–Fe(2′)	71.18(9)

filling of the one-electron energy levels. In the doubly charged species it was found that the maximum number of unpaired electrons which can contribute to the ground state is eight, when the one-electron energy levels are occupied in order of increasing energy.[1] In density functional theories this procedure, in principle, can lead to an excited rather than to the ground state. The best occupation number was therefore checked for various electronic configurations. The calculations showed that several one-electron configurations having the same total spin were possible. Nearly the same situation was encountered in the present calculations and the maximum number of unpaired electrons was found to be seven, corresponding to a $S = \frac{7}{2}$ total spin state. The closest excited configuration was computed to be $\approx 2000\ cm^{-1}$ (0.25 eV) higher in energy than the ground one.

Spin polarisation drastically affects the relative ordering of the energy levels near the Fermi energy. This is shown graphically in Fig. 7, where the configuration of minimum energy, among those allowed with seven unpaired electrons, is shown. In order to have higher spin states the anti-bonding band lying above the energy gap must be filled, giving rise to distinctly higher energy states.

Magnetic States.—The calculation of the multiplet structure is possible in density functional theory and it has been carried out successfully in a number of cases in the last few years.[5,16,33] When applied to describe weak-bonding interactions these calculations required the use of configuration interactions in order to compute quantitatively the magnetic exchange parameters appearing in equation (2), which describe energy separations between the magnetic levels of the order of kT ($\approx 300\ cm^{-1}$ or 0.04 eV at room temperature). In all of these calculations excited configurations having the same spin as the

Table 6 Mössbauer parameters for $[Fe_6(\mu_3\text{-}S)_8(PEt_3)_6][PF_6]$ **1**

T/K	δ*/ mm s^{-1}	ΔE_Q/ mm s^{-1}	ΔE_M/ kOe	Γ/ mm s^{-1}	A (%)
5.0	0.28	0.32	—	0.36	40
	0.51	−0.11	47.8	0.91	60
80.0	0.29	0.35	—	0.50	100

* Relative to room temperature α-Fe.

Table 7 Hellmann–Feynman forces[a] and total energies[b] computed for $[Fe_6(\mu_3\text{-}S)_8(PH_3)_6]^{n+}$

Molecule	Δ (%)	ΔE/eV
$[Fe_6(\mu_3\text{-}S)_8(PH_3)_6]^0$	+40	−18.7
$[Fe_6(\mu_3\text{-}S)_8(PH_3)_6]^+$	+25	−11.4
$[Fe_6(\mu_3\text{-}S)_8(PH_3)_6]^{2+}$	0	0
$[Fe_6(\mu_3\text{-}S)_8(PH_3)_6]^{3+}$	−26	14.6
$[Fe_6(\mu_3\text{-}S)_8(PH_3)_6]^{4+}$	−52	33.6

[a] Percentage variation with respect to the 2+ species: $\Delta\ (\%) = [F(n+) - F(2+)]/F(2+) \times 100$. [b] Energy difference from the energy of the 2+ species.

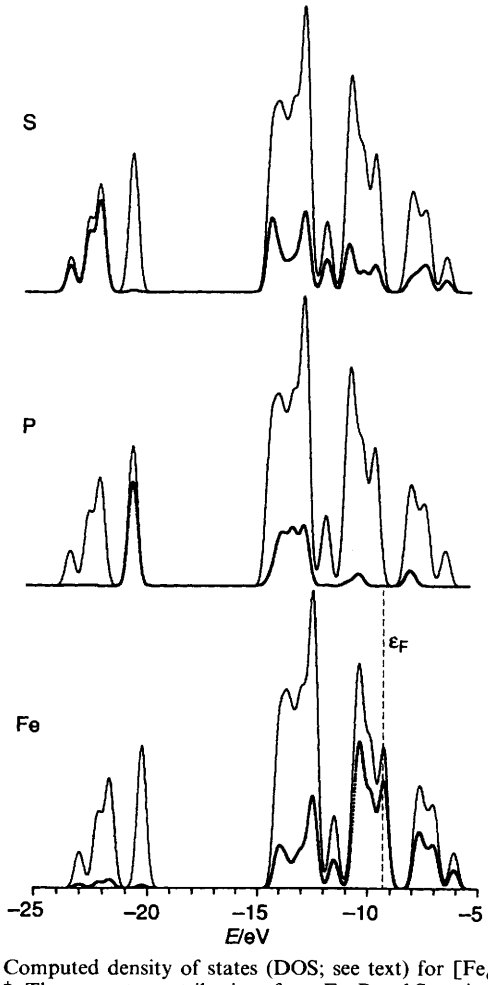

Fig. 6 Computed density of states (DOS; see text) for $[Fe_6(\mu_3\text{-}S)_8(PH_3)_6]^+$. The separate contributions from Fe, P and S are indicated

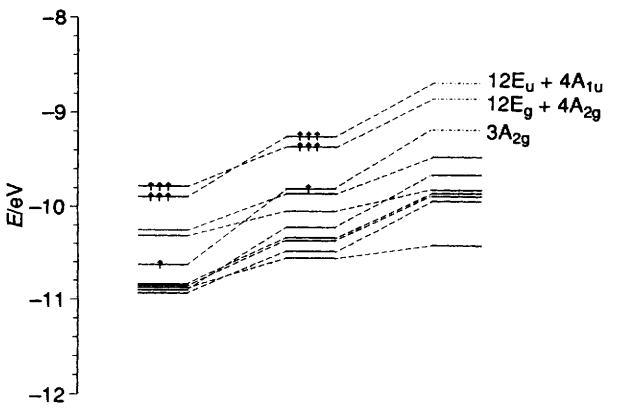

Fig. 7 Energy level scheme and occupation of the highest occupied and lowest unoccupied molecular orbitals of $[Fe_6(\mu_3\text{-}S)_8(PH_3)_6]^+$ in the $S = \frac{7}{2}$ state. The spin-restricted energy levels (in the centre) are compared with the spin-polarized ones (spin up levels on the left and spin down levels on the right)

ground configuration generally arose from charge-transfer states, well separated in energy from the ground state, and their contribution to the energy of the ground state was considered as a perturbation. In particular a formalism was developed[5] which, using only one Slater determinant built up on broken space and spin symmetries, included all the most relevant interactions in the calculation of the exchange coupling constants. The broken symmetry model has been applied to describe the magnetic structure of systems containing from two to four magnetically interacting centres, including the 4Fe–4S cubane-like systems, and corrections to the Heisenberg–Dirac–van Vleck Hamiltonian for delocalisation of the unpaired electrons onto two adjacent centres have been also evaluated. In all of the reported cases the metallic ions have been found in their high-spin states. Therefore a single orbital configuration was found to be accurate enough to describe the ground state of the isolated ions.

In our systems, the magnetic electrons are generated by low-spin ions. This means that more than one orbital configuration is likely to be used in the description of the ground magnetic state making the configuration interaction of overwhelming importance. This causes the quasi-orbital degeneracy in the MO calculations and, apart from the complexity of a broken symmetry calculation on a Fe_6 system, prevents us from making any quantitative determination of the multiplet structure. The only meaningfully information which can be extracted from the MO results is that spin states $S = \frac{7}{2}$ and 4 are allowed by the MO structures of $[Fe_6(\mu_3\text{-}S)_8(PH_3)_6]^+$ and $[Fe_6(\mu_3\text{-}S)_8(PH_3)_6]^{2+}$ respectively and that these states give the maximum spin multiplicity possible for a ground-state manifold.

Magnetic data for complex **1** indicate that the $S = \frac{7}{2}$ is indeed the ground state and that the excited magnetic states are not appreciably populated at room temperature. In order to correlate the MO results with the usual weak-bonding (exchange interaction) description [equation (2)] of the magnetic interactions, formal charges and spins should be assigned to the paramagnetic metal centres. Assigning a formal 2− charge to the sulfur atoms, the cluster is formed by five iron(III) and one iron(II) centres. The cluster can thus be assigned as a mixed-valence type of compound. According to the Mössbauer results the iron(III) centres should be low-spin, $S_i = \frac{1}{2}$. Therefore, a total $S = \frac{7}{2}$ spin state can arise only if the iron(II) centre is in the intermediate spin state $S = 1$ and the exchange coupling is ferromagnetic. This rather unusual spin state for iron(II) has been observed in complexes formed with strong ligand fields,[34] and, generally, in tetragonal-octahedral or square-pyramidal geometries.[35–38] Since complex **1** has to be classified in the mixed-valence class of substances, the Hamiltonian (2) cannot be applied rigorously to describe its magnetic properties and corrections for double-exchange phenomena should be added. This has been shown in several papers concerning di-, tri- and tetra-nuclear clusters.[39–42] An extension of the double-exchange formalism to Fe_6 cluster cores is underway.[43]

The iron atoms in complex **2** can be described, in the localised picture, as iron(III) centres. Iron(III) in square-pyramidal environments is generally found in the low-spin, $S = \frac{1}{2}$, or intermediate-spin, $S = \frac{3}{2}$, states.[44] Assigning $S_i = \frac{1}{2}$ spin to all of the iron(III) centres, no reasonable fit of the magnetic data can be obtained. In fact, since the room-temperature magnetic moment, $\mu_{eff} = 6.6\ \mu_B$, is definitely higher than that expected for six non-interacting $S_i = \frac{1}{2}$ spins, $\mu_{eff} = 4.2\ \mu_B$, a ferromagnetic spin coupling has to be operating between the low-spin centres in order to give an average magnetisation of $6.6\ \mu_B$. In this case the observed decrease of χT with decreasing temperature cannot be reproduced unless strong inter-cluster interactions are introduced, which cannot be justified on the basis of the structure of complex **2** in the solid state. The scattered-wave calculations have shown that a $S = 4$ spin state belongs to the ground spin manifold of a 2+ charged cluster. A total spin state of $S = 4$ cannot arise from the coupling of six $S_i = \frac{1}{2}$ (maximum $S = 3$), but can arise from the coupling of five $S_i = \frac{1}{2}$ with one $S_6 = \frac{3}{2}$, *i.e.* from the coupling of five iron(III) centres in the low-spin state and one in the intermediate-spin state. A fitting of the temperature variation of χT with temperature is possible using $J_{ij} = J$ (for any $i,j \neq 6$), $J_{i,6} = J'$ ($1 \leqslant i \leqslant 5$), and g as free parameters in equations (2) and (3), equation (4) being the function to be minimised. The results of the fitting are shown as the solid curve in Fig. 4(*a*). The best fit parameters are $g = 3.20(3)$, $J = 43.2(6)\ cm^{-1}$, and $J' = 169.6(3)\ cm^{-1}$, indicating that an antiferromagnetic interaction is operating between the iron centres. The measured g value is, however, unusually high. The magnetic properties of complex $[Fe_6(\mu_3\text{-}S)_8(PEt_3)_6][BPh_4]_2$, which differ from **2** because of the different counter anion, have been successfully interpreted using the same model. However, an anomaly in the χT *vs.* T curve in the temperature range 60–80 K was observed and assigned to a transition from the spin state $S_6 = \frac{3}{2}$ to the low-spin state, possibly modulated by vibronic effects.[1] Allowing for a similar spin transition in the present case leads to two distinct curves which best fit the magnetic data in the high- and low-temperature regions. The results of the fitting with this model are shown in Fig. 4(*b*) as solid curves. The high-temperature curve was computed using $g = 2.07(5)$, $J = 21.2(6)\ cm^{-1}$, and $J' = -330.7(4)\ cm^{-1}$. The low-temperature curve was computed using equations (2)–(4) with $S_i = \frac{1}{2}$ (for any i) and $J_{ij} = J$ (for any i,j); the best-fit parameters were $g = 2.07(2)$ and $J = 0.2(8)\ cm^{-1}$. These results are in qualitative agreement with those obtained for $[Fe_6(\mu_3\text{-}S)_8(PEt_3)_6][BPh_4]_2$. The description of the magnetic structure of **2** suffers, in principle, from the same defects as the localised description of the magnetic properties of mixed-valence species, which however, was found useful to characterise the systems empirically.[45,46] In the molecular structure of **2** no appreciable difference between the iron centres in the cluster is seen. Although not crystallographically equivalent, they lie in equal chemical environments. The $S = \frac{3}{2}$ spin state which we have localised on one of the iron centres should therefore be delocalised over the whole cluster. We call this system a mixed-spin-state complex.

Redox Behaviour.—The Fe_6S_8 core was found[14] to undergo several one-electron reduction steps according to the scheme reported below, the species $[Fe_6S_8]^0$ and $[Fe_6S_8]^{4+}$ being short lived.

$$[Fe_6S_8]^{4+} \underset{-e^-}{\overset{+e^-}{\rightleftharpoons}} [Fe_6S_8]^{3+} \underset{-e^-}{\overset{+e^-}{\rightleftharpoons}} [Fe_6S_8]^{2+} \underset{-e^-}{\overset{+e^-}{\rightleftharpoons}} [Fe_6S_8]^{+} \underset{-e^-}{\overset{+e^-}{\rightleftharpoons}} [Fe_6S_8]^{0}$$

The electronic structure of the uncharged species can easily be computed, with our model molecule, by adding one electron to $[Fe_6(\mu_3\text{-}S)_8(PEt_3)_6]^+$. Upon removing up to two electrons from $[Fe_6(\mu_3\text{-}S)_8(PEt_3)_6]^{2+}$, the 3+ and 4+ species are easily obtained. In order to rationalise the electrochemical behaviour we have to compare the computed relative stabilities of the species. This can, in principle, be done by comparing the computed total energies. This procedure is not rigorous when the scattered-wave approximation is used to solve the molecular Hamiltonian, as the computed energies are dependent on the muffin-tin partition of the molecular space. In the present case this could be of minor importance since the space partitioning is constant over all the systems. A more serious problem, in the present case, is given by the spin structure of the complex which cannot be represented by one single Slater determinant. Methods of calculations not based on density functional theories would require extensive configuration interaction to treat this problem, thus making calculations prohibitive as far as the computer time is concerned. In order to try to estimate the relative stabilities of the oxidation states we, therefore, resorted to compute the total energies and the Hellmann–Feynman forces on the iron centres in the high-spin states of the various molecules. The results of the calculations are collected in Table 7. The Hellmann–Feynman forces were computed according to the procedure described in the Computational section.

The force criterion[29] was recently used to characterise the structural features of cobalt–sulfur clusters;[6,15] in particular the parent cluster $[Co_6(\mu_3\text{-}S)_8(PEt_3)_6]^{2+}$ was predicted to have a stable structure[15] while only the 0 and 1+ charged species were isolated in the solid state. Some of us[47] have recently succeeded in isolating the 2+ charged species in the form $[Co_6(\mu_3\text{-}S)_8(PEt_3)_6][I_7]_2$.

Contrary to previous findings for the cobalt clusters, the forces computed for the iron clusters showed a strong relative variation upon removing and adding one electron. The largest force is computed for the 0 species and the force decreases on decreasing the total number of electrons. This can be related to the progressive decrease of occupied anti-bonding orbitals. On passing from the 2+ to the 1+ species the force increases by 25%. As a consequence a distortion of the molecular structure is expected. If we compare, for example, the mean Fe–Fe distances [2.62(1) and 2.64(2) Å in **2** and **1** respectively] they can be considered equal within experimental error indicating that the computed increase of the force exerts a minor effect on the structure of the cluster. On passing to the 3+ charged species a 25% decrease in the force with respect to the 2+ species is computed and a 50% decrease is computed for the 4+ species. If geometrical deformations should occur in order to stabilise different species, these should be accessible for the 3+ species, while a larger deformation should occur in order to stabilise the 4+ species. Total energies stabilise the lower oxidation states. These two parameters should, therefore, exclude the possibility of obtaining the 4+ species as a stable complex, while nothing can safely be concluded for the 3+ and 0 species.

Conclusion

Sulfide clusters of general formula $[Fe_6S_8(PEt_3)_6]^{n+}$ ($n = 1$ or 2) can be described as integer or mixed-valence systems depending on the charge n. For $n = 2$ the iron centres possess the formal oxidation state 3+, for $n = 1$ five irons are in the formal oxidation state 3+ and one in the 2+. Their magnetic properties can be interpreted within the usual Heisenberg–Dirac–van Vleck exchange spin Hamiltonian only by assuming that some iron centre is present in an intermediate spin state thus leading to the general description of these clusters as mixed-valence and mixed-spin-state systems.[1] To the best of our knowledge, these are the first examples of such systems. This description is bound to the Heisenberg–Dirac–van Vleck model of the exchange interaction, which constitutes the simplest approach to the magnetic structure of the cluster. In this model the interacting magnetic electrons are considered as localised onto different sites in the molecule and therefore having a small delocalisation to the chalcogen ligand. A slightly more general approach which takes into account the equivalence of the six iron atoms is currently being developed.[43] A more accurate description should, indeed, be based on full MO calculations in which the contribution of the chalcogen to the magnetic exchange is taken into account. Unfortunately this approach is unfeasible for such large systems, at present.

Density functional calculations in the scattered-wave approximation have been found to be helpful in rationalising the magnetic structure of the clusters. In particular the correct spin of the ground state has been predicted not only for $[Fe_6S_8(PEt_3)_6]^+$ **1** ($S = \frac{7}{2}$), but also for $[Co_6S_8(PEt_3)_6]$ ($S = 0$) and $[Co_6S_8(PEt_3)_6]^+$ ($S = \frac{1}{2}$).[6] Calculations of the same kind also allow an interpretation of the temperature behaviour of the magnetic susceptibility of $[Fe_6S_8(PEt_3)_6]^{2+}$ **2**, whose magnetic states, in the Heisenberg–Dirac–van Vleck picture, arise from the interaction of five low-spin iron(III) centres ($S = \frac{1}{2}$) with one intermediate-spin iron(III) centre ($S = \frac{3}{2}$), and a rationalisation of the relative stabilisation of the various spin states. On the same grounds, the magnetic states of the monopositive cation **1** arise from a ferromagnetic coupling between five iron(III) low-spin centres and one iron(II) centre in the intermediate ($S = 1$) spin state. We suggest **1** is classified as a mixed-valence mixed-spin-state system.

Clusters, like the present ones, in which the diamagnetic ligands bridging the metallic paramagnetic centres can strongly influence the magnetic properties, can produce new solids with unexpected physicochemical properties. The present results show that the magnetic behaviour can also be subtly influenced by the nature of the counter ion. Further investigations are necessary for a more detailed understanding of the correlation between the magnetic and electronic and geometrical structures of these systems.

Acknowledgements

Thanks are expressed to Dr. A. Caneschi, Università di Firenze, for performing the magnetic measurements on the SQUID apparatus and to Professor D. Gatteschi, Università di Firenze, for helpful discussions. Thanks are also due to Mr. F. Cecconi, C.N.R. di Firenze, for the synthesis of the complexes and to Mr. M. Fontanelli, Università di Firenze, for computer assistance. M. G. U. thanks the European Community for a research grant.

References

1 Part 3, A. Bencini, M. G. Uytterhoeven and C. Zanchini, *Int. J. Quantum Chem.*, 1994, **52**, 903.
2 A. Bencini and S. Midollini, *Coord. Chem. Rev.*, 1992, **120**, 87.
3 B. Hessen, T. Siegrist, T. Palstra, S. M. Tanzler and M. L. Steigerwald, *Inorg. Chem.*, 1993, **32**, 5165.
4 D. Gatteschi, B. Tsukerblatt, A. L. Barra, L. C. Brunel, A. Müller and J. Döring, *Inorg. Chem.*, 1993, **32**, 2114.
5 L. Noodleman and D. A. Case, *Adv. Inorg. Chem.*, 1992, **38**, 423.
6 A. Bencini, C. A. Ghilardi, A. Orlandini, S. Midollini and C. Zanchini, *J. Am. Chem. Soc.*, 1992, **114**, 9898.
7 A. Bencini, S. Midollini and C. Zanchini, *Inorg. Chem.*, 1992, **31**, 2132.
8 A. Agresti, M. Bacci, F. Cecconi, C. A. Ghilardi and S. Midollini, *Inorg. Chem.*, 1985, **24**, 689.
9 O. Kahn, *Molecular Magnetism*, VCH, New York, 1993.
10 A. Bencini and D. Gatteschi, *Electron Paramagnetic Resonance of Exchange Coupled Systems*, Springer, Berlin, 1990.
11 R. G. Parr and W. Yang, *Density-Functional Theory of Atoms and Molecules*, Clarendon Press, Oxford, 1989.
12 K. H. Johnson, *Adv. Quantum Chem.*, 1973, **7**, 143.
13 J. C. Slater, *The Self-consistent Field for Molecules and Solids*, McGraw-Hill, New York, 1974.
14 F. Cecconi, C. A. Ghilardi, S. Midollini, A. Orlandini and P. Zanello, *J. Chem. Soc., Dalton Trans.*, 1987, 831.

15 G. G. Hoffman, J. K. Bashkin and M. Karplus, *J. Am. Chem. Soc.*, 1990, **12**, 8705.
16 A. Bencini, *J. Chem. Phys.*, 1989, **86**, 763.
17 A. Bianchi, P. Dapporto, G. Fallani, C. A. Ghilardi and L. Sacconi, *J. Chem. Soc., Dalton Trans.*, 1973, 641.
18 N. Walker and D. Stuart, *Acta Crystallogr., Sect. A*, 1983, **39**, 158.
19 *International Tables for X-Ray Crystallography*, Kynoch Press, Birmingham, 1974, vol. 4, p. 99.
20 R. F. Stewart, E. R. Davidson and W. T. Simpson, *J. Chem. Phys.*, 1965, **42**, 3175.
21 Ref. 18, p. 149.
22 G. M. Sheldrick, SHELX 76, System of Computing Programs, University of Cambridge, Cambridge, 1976.
23 C. K. Johnson, ORTEP, Report ORNL-5138, Oak Ridge National Laboratory, Oak Ridge, TN, 1976.
24 D. A. Case and M. Karplus, *Chem. Phys. Lett.*, 1976, **39**, 33.
25 M. Cook and M. Karplus, *J. Chem. Phys.*, 1980, **72**, 7.
26 D. A. Case, M. Cook and M. Karplus, *J. Chem. Phys.*, 1980, **73**, 329.
27 K. Schwartz, *Phys. Rev. B*, 1972, **5**, 2466.
28 (*a*) J. C. Slater, *Int. J. Quantum Chem.*, 1973, **57**, 333. (*b*) J. G. Norman, jun., *Mol. Phys.*, 1976, **31**, 1191.
29 *The Force Concept in Chemistry*, ed. B. M. Deb, Van Nostrand-Reinhold, New York, 1974, vol. 4.
30 P. W. Anderson, in *Magnetism*, eds. G. T. Rado and H. Suhl, Academic Press, New York, 1963, vol. 1.
31 P. Gütlich, R. Link and A. Trautwein, in *Mössbauer Spectroscopy and Transition Metal Chemistry*, Springer-Verlag, Berlin, 1978; H. H. Wickman, in *Mössbauer Effect Methodology*, ed. I. J. Gruwerman, Plenum Press, New York, 1962, vol. 2.
32 F. Del Giallo, F. Pieralli, L. Fiesoli and G. Spina, *Phys. Rev. Lett. Sect. A*, 1983, **96**, 141.
33 T. Ziegler, *Chem. Rev.*, 1991, **91**, 651.
34 P. N. Hawker and M. V. Twigg, in *Comprehensive Coordination Chemistry*, eds. G. Wilkinson, R. D. Gillard and J. A. McCleverty, Pergamon Press, Oxford, 1987, vol. 4, p. 1289.
35 K. D. Hodges, R. D. Wollmann, E. K. Barefield and D. N. Hendrickson, *Inorg. Chem.*, 1977, **16**, 2746.
36 S. Kock, R. H. Holm and R. B. Frankel, *J. Am. Chem. Soc.*, 1975, **97**, 6714.
37 M. Bacci, S. Midollini, P. Stoppioni and L. Sacconi, *Inorg. Chem.*, 1973, **12**, 1801.
38 M. Bacci and C. A. Ghilardi, *Inorg. Chem.*, 1974, **13**, 2398.
39 G. Blondin and J.-J. Girerd, *Chem. Rev.*, 1990, **90**, 1359.
40 E. Münck, V. Papaefthymiou, K. K. Surerus and J.-J. Girerd, *ACS Symp. Ser.*, 1988, **372**, 302.
41 B. S. Tsukerblat, M. Belinskii and V. E. Fainzil'berg, *Sov. Chem. Rev.*, 1987, **9**, 339.
42 M. Belinskii, *Chem. Phys.*, 1993, **173**, 27; **176**, 37.
43 A. Bencini, S. M. Ostrovsky, A. V. Palii, B. S. Tsukerblat and M. G. Uytterhoeven, unpublished work.
44 S. M. Nelson, in *Comprehensive Coordination Chemistry*, eds. G. Wilkinson, R. D. Gillard and J. A. McCleverty, Pergamon Press, Oxford, 1987, vol. 4, p. 217.
45 G. C. Papaefthymiou, E. J. Laskowski, S. Frota-Pessoa, R. B. Frankel and R. H. Holm, *Inorg. Chem.*, 1982, **21**, 1723.
46 P. Barbaro, A. Bencini, I. Bertini, F. Briganti and S. Midollini, *J. Am. Chem. Soc.*, 1990, **112**, 7238.
47 A. Bencini, F. Cecconi, G. A. Ghilardi, A. Orlandini and S. Midollini, unpublished work.

Received 7th September 1994; *Paper* 4/05455E